Applied Catalysis B: Environmental 97 (2010) 120–126

Contents lists available at ScienceDirect

Applied Catalysis B: Environmental

journal homepage: www.elsevier.com/locate/apcatb

Catalytic combustion of ethyl acetate and nano-structural changes of ruthenium catalysts supported on tin oxide

Naoto Kamiuchi, Tomohiro Mitsui, Hiroki Muroyama, Toshiaki Matsui, Ryuji Kikuchi[1], Koichi Eguchi*

Department of Energy and Hydrocarbon Chemistry, Graduate School of Engineering, Kyoto University, Nishikyo-ku, Kyoto 615-8510, Japan

ARTICLE INFO

Article history:
Received 7 October 2009
Received in revised form 1 March 2010
Accepted 25 March 2010
Available online 31 March 2010

Keywords:
Ruthenium
Tin oxide
Catalyst
Catalytic combustion
Ethyl acetate
Chemical interaction
TEM

ABSTRACT

Correlation between the catalytic activity and the nano-structure of ruthenium catalyst supported on tin oxide was investigated. As-calcined Ru/SnO_2 catalyst exhibited high catalytic activity for ethyl acetate combustion despite its low surface area of ca. 5.0 $m^2\ g^{-1}$. The catalytic activity was degraded by the reduction treatment at 400 °C, whereas it was partially restored by the subsequent reoxidation treatment at 400 °C. To elucidate the variation in the catalytic activity, the ruthenium catalysts heat-treated under reductive or oxidative condition were characterized by X-ray diffraction (XRD), X-ray photoelectron spectroscopy (XPS), and transmission electron microscopy (TEM). In the as-calcined catalyst, it was revealed that the fine particles with the small contact angles were well-dispersed on the surface of tin oxide support. In the deactivated catalyst treated at 400 °C under a reductive atmosphere, the large particles of intermetallic compounds with the core–shell structure were clearly observed. On the other hand, upon the reoxidation treatment at 400 °C the particles with the core–shell structure disappeared accompanied with the appearance of the nano-sized particles. Accordingly, it was clarified that the catalytic activity was strongly influenced by the structural changes of active sites such as sintering and redispersion.

1. Introduction

The catalysts composed of precious metals have been applied to a large number of chemical reactions. They are very useful and indispensable for human life due to their high catalytic activities. The precious metals, however, are generally expensive because of their limited prospect. Thereby, it is of significant importance to make an effective use of them. The metal oxide particles with high surface area such as Al_2O_3 and SiO_2 have been used as supports so as to disperse precious metals. This technique also leads to other advantages such as the suppression of the aggregation of metal particles and the improvement of the thermal stability. Furthermore, in 1978, Tauster et al. discovered the interesting phenomenon named as SMSI (strong metal–support interaction) in the case of platinum catalysts supported on several kinds of metal oxides [1–4]. It is well-known that this phenomenon strongly affects the gaseous adsorption property. Since then, a number of studies regarding to the significant role of the support materials on the catalytic reaction have been reported. The catalysts of Pd/SnO_2 [5–8], Pt/SnO_2 [9–14], and Pt/Co_3O_4 [15] are used as the combustion catalysts for VOCs (volatile organic compounds) and the electrocatalysts for PEFC (polymer electrolyte fuel cell). It was revealed that the chemical interaction between metal particles and support affected the catalytic activity and depended on the pretreatment conditions such as temperature, atmosphere, and time. Thus, the control of the chemical interaction at the interface between metal particles and support enables to improve the catalytic activity and the catalyst life.

The ruthenium, one of the precious metals, is also used as a catalyst for many chemical reactions; the olefin metathesis reactions [16–18], the hydrogenation of unsaturated compounds [19,20], the ammonia synthesis [21–23], the heterogeneous oxidation of alcohols [24], the low temperature oxidation of VOCs [25–27], and so on. Recently, we reported that the ruthenium catalysts supported on CeO_2, ZrO_2, and SnO_2 showed the high catalytic activities for the oxidation of ethyl acetate, acetaldehyde, and toluene [28]. In addition, the catalytic activities were strongly influenced by the pretreatment in hydrogen. It was suggested for the high activities that the strong chemical interaction between ruthenium and metal oxide supports was responsible. However, the nano-structural changes and the effect of reoxidation treatment on the catalytic activities have not been elucidated sufficiently. In this study, therefore, the correlation between the nano-structure and the catalytic activities for the oxidation of ethyl acetate was

* Corresponding author. Tel.: +81 75 383 2519; fax: +81 75 383 2520.
E-mail address: eguchi@scl.kyoto-u.ac.jp (K. Eguchi).
[1] Present address: Department of Chemical System Engineering, The University of Tokyo, 7-3-1 Hongo, Bunkyo-ku, Tokyo 113-8656, Japan.

0926-3373/$ – see front matter © 2010 Elsevier B.V. All rights reserved.
doi:10.1016/j.apcatb.2010.03.031

Table 1
Heat-treatment of 1.0 wt.% Ru/SnO_2 and 10 wt.% Ru/SnO_2.

Sample name	Heat-treatment
S-1	As-calcined
S-2	Reduction[a] at 400 °C for 0.5 h
S-3	Reduction at 400 °C for 0.5 h, followed by oxidation[b] at 400 °C for 0.5 h
S-4	Reduction at 400 °C for 0.5 h, followed by oxidation[b] at 400 °C for 5 h

[a] Reduction atmosphere: 10% H_2/N_2.
[b] Oxidation atmosphere: air.

investigated for Ru/SnO_2 catalyst heat-treated in several conditions.

2. Experimental

2.1. Catalyst preparation

The ruthenium catalysts supported on tin oxide were prepared by the conventional impregnation method. The solution of $Ru(NO_3)_3$ (Tanaka Kikinzoku Kogyo) and the powder of tin oxide (Wako Pure Chemical Industries, Ltd.) calcined at 800 °C for 5 h in air were used as a ruthenium source and a support, respectively. The loading amount of ruthenium was fixed at 1.0 wt.% and 10 wt.%. The latter catalyst with heavy loading amount was prepared for clarifying the structural change between metal and support by X-ray diffraction and X-ray photoelectron spectroscopy. After SnO_2 powder was impregnated with $Ru(NO_3)_3$, the mixture was kept on a steam bath at 80 °C to evaporate the solution. Subsequently, the resulting powder was calcined at 400 °C for 0.5 h in air. A part of this as-calcined catalyst denoted as S-1 was heat-treated in several conditions summarized in Table 1.

2.2. Catalytic combustion of ethyl acetate

A fixed-bed flow reactor made of quartz tubing of 8 mm inner diameter was used, and the prepared catalyst (600 mg) was set in the reactor. All catalysts with 1.0 wt.% Ru were tabletted and pulverized into 10–26 mesh before catalytic reaction tests. A gaseous mixture composed of 0.1% ethyl acetate and 99.9% air was fed with a flow rate of 100 ml min^{-1} (space velocity: 10,000 l kg^{-1} h^{-1}). The outlet gas composition was analyzed by an on-line gas chromatograph with a thermal conductivity detector (TCD) (VARIAN, CP-4900) and a flame ionization detector (FID) (Shimadzu, GC-8A). The temperature was continuously raised from room temperature up to 300 °C at a heating rate of 100 °C h^{-1}. The measurements were started soon after the concentration of ethyl acetate and CO_2 in the outlet gas became stable.

2.3. Characterization by XRD, XPS, and FE-TEM

The phases of ruthenium catalysts were characterized by X-ray diffraction (XRD) (Rigaku Rint 1400, X-ray diffractometer with Cu Kα radiation). X-ray photoelectron spectroscopy (XPS) (Shimadzu ESCA-3400, Mg Kα radiation) measurements were carried out so as to evaluate the surface electronic state and to analyze the surface atomic ratio of Ru/Sn. The reduction treatment for S-2 was conducted in the pretreatment chamber which enables to analyze the sample without exposure to air. All binding energies were calibrated with reference to the Sn $3d_{5/2}$ peak (487.1 eV). The analyses of ruthenium species in 1.0 wt.% Ru/SnO_2 catalysts by XRD and XPS were hard due to the low loading amount of ruthenium. Therefore, 10 wt.% Ru/SnO_2 catalysts were used for the characterization by X-ray apparatuses. The nano-structure and electronic state of ruthenium particles might be affected by the loading amount,

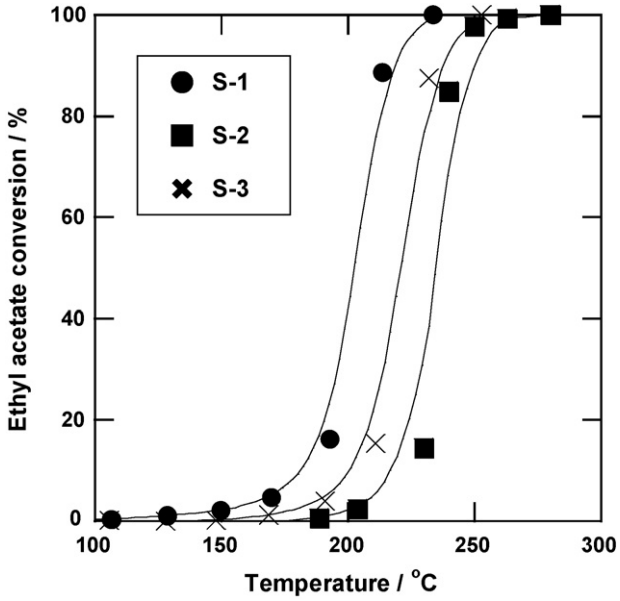

Fig. 1. Ethyl acetate conversion as a function of temperature over 1.0 wt.% Ru/SnO_2 treated with calcinations in various conditions. Reaction conditions: ethyl acetate, 0.1%; air, 99.9%; S.V. = 10,000 l kg^{-1} h^{-1}.

while it was reported that the properties of 1.0 wt.% Pt/SnO_2 was essentially the same as those of 20 wt.% Pt/SnO_2 [10,11]. Thus, the microstructure and electronic state of ruthenium species in 1.0 wt.% Ru/SnO_2 will be same with those in 10 wt.% Ru/SnO_2.

Field emission transmission electron microscopy (FE-TEM) was used in order to observe the morphology and lattice images of the catalysts. All catalysts were dispersed in ethanol by ultrasonic wave and dropped on carbon coated copper microgrids. FE-TEM digital images were obtained by using Philips CM200 FEG equipped with a field emission electron gun, a CCD camera, digital micrograph software (Gatan), and an electron energy analyzer for energy loss spectroscopy (EELS).

3. Results and discussion

3.1. Ethyl acetate combustion

In the earlier work, Mitsui et al. reported that the catalytic activities for ethyl acetate combustion over 1.0 wt.% Ru/SnO_2 were deteriorated after the reduction treatment [28]. On the other hand, the restoration of catalytic activities for CO oxidation was verified in the case of Pt/SnO_2 after the reoxidation treatment [11]. From these perspective, the catalytic activities for ethyl acetate combustion over 1.0 wt.% Ru/SnO_2 were examined as shown in Fig. 1. Over the as-calcined catalyst (S-1), the oxidation of ethyl acetate started at ca. 150 °C followed by the steep increase in conversion up to 100% at 230 °C though the BET surface area of as-calcined Ru/SnO_2 catalyst was reported to be 4.9 m^2 g^{-1} [28]. The catalytic activity of the as-calcined catalyst was degraded by the reduction treatment at 400 °C. The ignition temperature for the reduced catalyst (S-2) was ca. 200 °C. The deteriorated catalytic activity was recovered to some extent after the reoxidation treatment at 400 °C for 0.5 h (S-3).

3.2. Characterization by XRD

The analysis by X-ray diffraction was performed for 10 wt.% Ru/SnO_2 catalysts from S-1 to S-4. As can be seen in Fig. 2, the RuO_2 and SnO_2 phases were detected in the as-calcined catalyst (S-1).

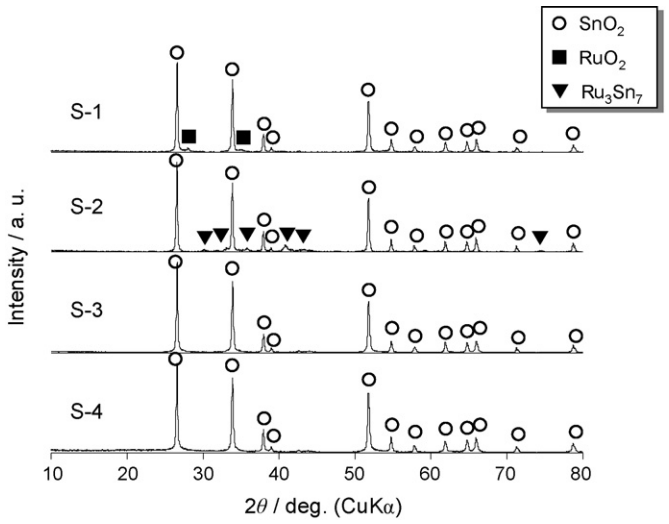

Fig. 2. XRD patterns of 10 wt.% Ru/SnO_2 (S-1 to S-4).

Therefore, the ruthenium species are in the oxidized state after the calcination treatment at 400 °C. On the other hand, the diffraction pattern consisted of the intermetallic compound (Ru_3Sn_7) and SnO_2 phases in the case of the reduced S-2 catalyst. This result implies the occurrence of the reduction of ruthenium species and subsequent dissolution into SnO_2 particle in a reducing atmosphere. In the case of Pt/SnO_2 catalyst, it was reported that the SnO_2 support was easily reduced even at low temperature such as 400 °C and the intermetallic compound phases of PtSn and Pt_3Sn were formed [10]. It is of interest that the phase derived from ruthenium species was not detected in the reoxidized catalysts (S-3 and S-4) regardless of their high loading amount of ruthenium. Two reasons can be considered for this result. One is that the particles of ruthenium species are too small to be detected by X-ray apparatus, and the other is the sublimation of RuO_2 caused by the reoxidation treatment at the high temperature. It is well-known that RuO_2 is sublimed at 900 °C or higher temperatures [29]. In this experiment, however, the temperature of the reoxidation treatment was 400 °C. Thereby, it is suggested that the ruthenium oxide particles would be highly redispersed in the reoxidized catalysts.

3.3. Characterization by XPS

The surface electronic state of 10 wt.% Ru/SnO_2 catalysts was evaluated by using an XPS apparatus equipped with a pretreatment chamber. The samples exposed to air for 1 day, 1 week, 2 weeks, and 3 weeks after the reduction in the pretreatment chamber were also analyzed in addition to the samples summarized in Table 1. The spectra of Ru 3d and Sn 3d were depicted in Fig. 3(a) and (b), respectively. The binding energies of RuO_2 (Ru^{4+}) and metallic Ru (Ru^0) have been reported to be 280.7 eV and 280.1 eV, respectively [30]. Accordingly, the peak at 280.7 eV in the Ru 3d spectrum of S-1 was assigned to the ruthenium species in the oxidized state such as RuO_2, and the peak at ca. 280.0 eV of S-2 was ascribed to metallic ruthenium. The negative shift of Ru 3d peak indicates that the ruthenium in the oxidized state was sufficiently reduced to the metallic state by the reduction treatment at 400 °C. Even after the exposure to air for 3 weeks, no significant changes of Ru 3d spectra were confirmed for S-2. After the reoxidation treatment at high temperatures, however, the peaks of Ru 3d spectra were shifted to the oxidized state (280.7 eV). From the small shoulder peak of S-2 shown in Fig. 3(b), it is apparent that SnO_2 in S-1 was partially reduced to SnO (486.0 eV) and Sn (485.0 eV) by the reduction treatment at 400 °C (S-2) [30]. Furthermore, the reduced tin species in S-2 were gradually reoxidized upon the exposure to air and the heat-treatments at 400 °C for 0.5 h (S-3) and 5 h (S-4) in air. From these measurements, it was clarified that the surface electronic states of Ru and Sn were returned to the initial states of S-1 by the reoxidation treatments after the reduction at 400 °C.

The surface composition ratio of Ru/Sn in 10 wt.% Ru/SnO_2 catalysts was evaluated from the peak area of Ru $3d_{5/2}$ and Sn $3d_{5/2}$ spectrum. The results of the surface atomic ratio were summarized in Table 2. The surface atomic ratio of 10 wt.% Ru/SnO_2 catalyst calcined at 400 °C was estimated to be 0.40, whereas that of the cat-

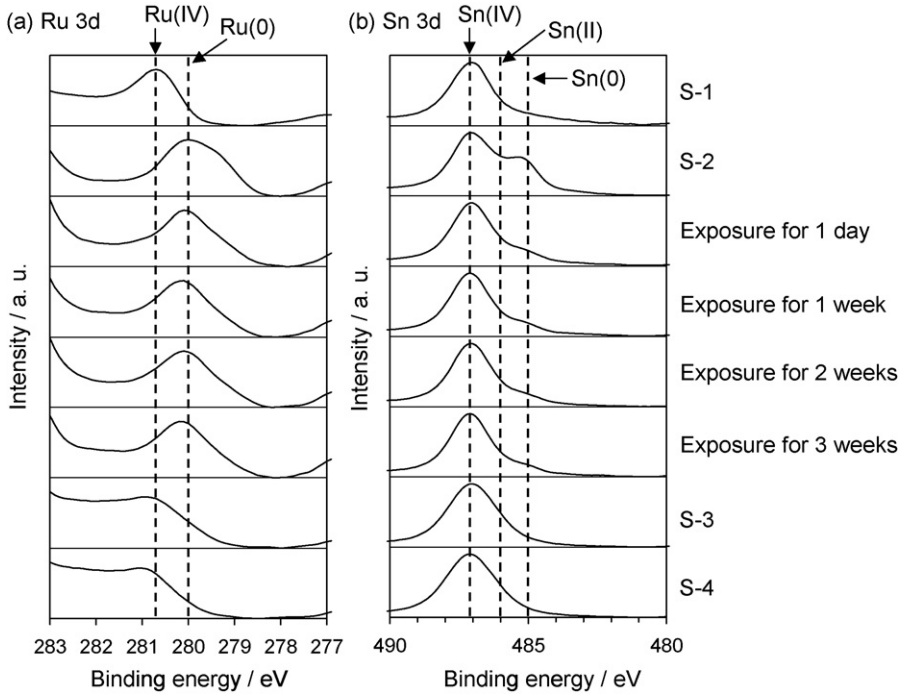

Fig. 3. XPS spectra of 10 wt.% Ru/SnO_2 treated in several conditions: (a) Ru 3d and (b) Sn 3d.

Table 2
Surface atomic ratio (Ru/Sn) of 10 wt.% Ru/SnO_2 treated under several conditions.

Condition of pretreatment	Atomic ratio (Ru/Sn)
As-calcined	0.40
Reduced at 400 °C in situ	0.17
Exposed in air for 1 day after reduction at 400 °C	0.11
Exposed in air for 3 weeks after reduction at 400 °C	0.097

alyst reduced in hydrogen at 400 °C for 0.5 h was 0.17. This decrease in Ru/Sn ratio is attributed to the particle growth and the formation of the intermetallic compound by the reduction treatment. The Ru/Sn ratios after the exposure to air for 1 day and 3 weeks were 0.11 and 0.097, respectively. Thus, the composition of ruthenium on the top surface gradually decreased with time. The decrease of the surface ruthenium species appears to be related with the variation of the Sn spectra as shown in Fig. 3(b).

3.4. Microscopic observation of Ru/SnO_2 catalysts

Fig. 4 shows the typical FE-TEM image of 1.0 wt.% Ru/SnO_2 catalyst calcined at 400 °C (S-1). Extremely thin and fine particles (ca. 2 nm) with the small contact angles indicated by the white arrows were well-dispersed on the surface of support. The latter particles are composed of a few atomic layers, indicating that the RuO_2 particles are under the strong chemical interaction with SnO_2 supports. A plan view TEM images of S-1 are shown in Fig. 5. Several rectangular areas, indicated by the white arrows in the enlarged image (Fig. 5(b)), correspond to the thin RuO_2 particles in the well-crystallized state. The rectangle shape may result from the crystal structure of tetragonal [31].

The TEM images of 1.0 wt.% Ru/SnO_2 catalyst reduced at 400 °C (S-2) are shown in Fig. 6. From the photograph, it is obvious that the large particles with the unique core–shell structure existed on the top surface of SnO_2 particles. The core–shell structure was further investigated from the high magnification image. As can be seen in Fig. 7, the core part was well-crystallized one with the lattice fringe attributable to Ru_3Sn_7 (3 1 0). On the other hand, the shell part was in the amorphous state. The mapping of Sn atom was examined by EELS so as to elucidate the atomic composition of the core–shell structure. FE-TEM photograph of the particles with the core–shell

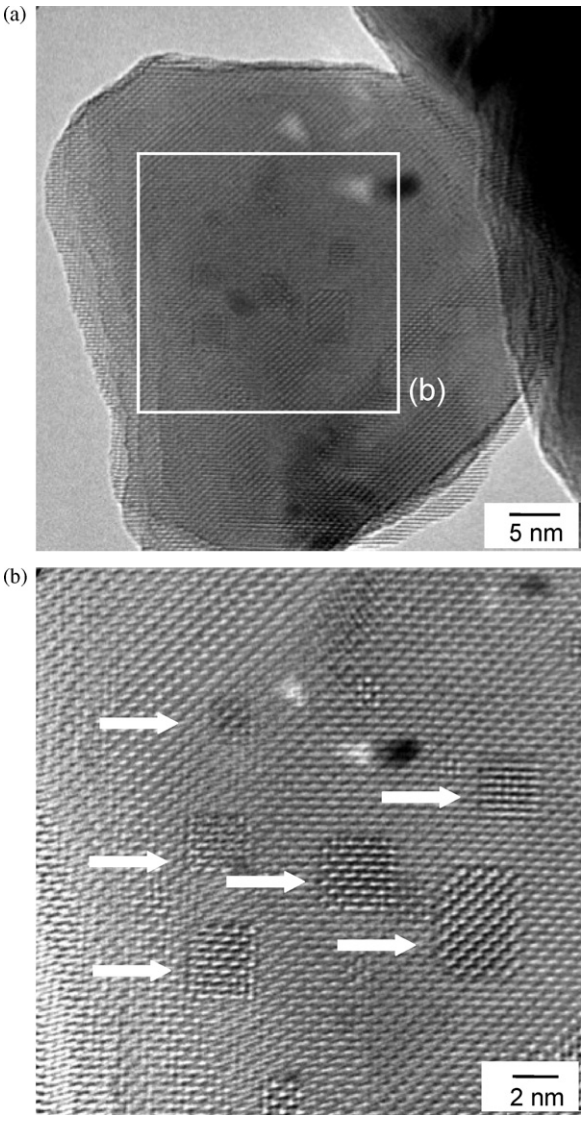

Fig. 5. Plan view images of 1.0 wt.% Ru/SnO_2 calcined at 400 °C for 0.5 h in air (S-1).

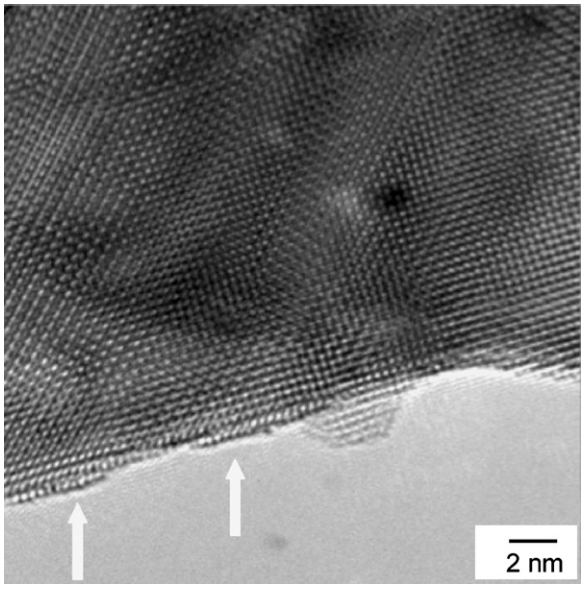

Fig. 4. A profile view image of 1.0 wt.% Ru/SnO_2 calcined at 400 °C for 0.5 h in air (S-1).

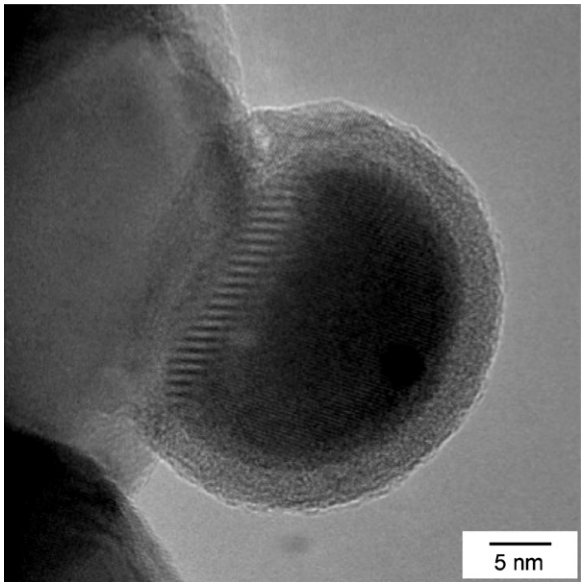

Fig. 6. TEM image of 1.0 wt.% Ru/SnO_2 reduced in 10% H_2/N_2 at 400 °C for 0.5 h (S-2).

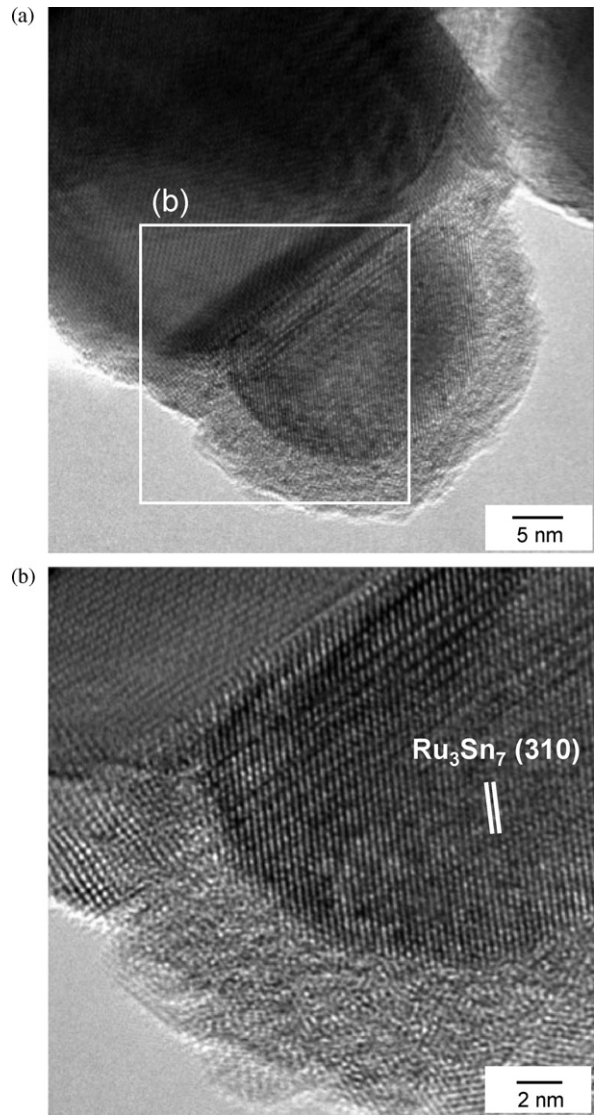

Fig. 7. High resolution images of 1.0 wt.% Ru/SnO_2 reduced in 10% H_2/N_2 at 400 °C for 0.5 h (S-2).

structure and the corresponding mapping image of Sn atom are shown in Fig. 8(a) and (b), respectively. The bright part in Fig. 8(b) corresponds to the area including Sn atom. Thus, it is clear that the shell part consists of larger amount of Sn atoms as compared with the core part.

The structural change induced by reoxidation treatment was also investigated by TEM. The TEM images of 1.0 wt.% Ru/SnO_2 catalyst reoxidized at 400 °C for 0.5 h in air (S-3) are shown in Fig. 9. After the reoxidation treatment, the particles with the core–shell structure disappeared, whereas the particles in the polycrystalline state were observed. In order to clarify this structural change, 10 wt.% Ru/SnO_2 catalyst reoxidized at 400 °C for 5 h (S-4) was also observed (Fig. 10). It was noteworthy that the fine particles with the mean diameter of 3 nm were redispersed on the surface of support. These results imply that the redispersion of the fine particles proceeds gradually by the reoxidation treatment.

3.5. The correlation between the catalytic activity and the nano-structure

Throughout the experiments mentioned above, it was revealed the reduction–oxidation treatments sensitively affect the nano-structure and the catalytic activities. In the case of as-calcined catalyst (S-1), the existence of thin and fine RuO_2 particles highly-dispersed on the surface of SnO_2 support indicates the strong chemical interaction at the interface between these two components. Such unique morphology of RuO_2 particles will lead to the high catalytic activity for ethyl acetate combustion.

The deterioration of the catalytic activity was induced by the reduction treatment at 400 °C. In the reduced sample (S-2), the formation of the particles with core–shell structure was observed from high-magnified TEM images. Furthermore, it was revealed by the XRD analysis and the lattice fringe in TEM photograph that the size of particles consisting of the intermetallic compounds (Ru_3Sn_7) was larger than that of RuO_2 particles in S-1. Although the spherical ruthenium particles have been reported by many researchers in the reduced catalysts supported on Al_2O_3 [32], TiO_2 [33], MgO [34,35], and so on, the particles with the core–shell structure have not been found in the Ru/oxide system. Recently, we found the similar core–shell structure in the reduced Pt/SnO_2 catalyst [10,11]. In the case of Pt/SnO_2 catalyst, it was concluded that the particles with the core–shell structure was formed by the phase separation of tin species from the intermetallic compound

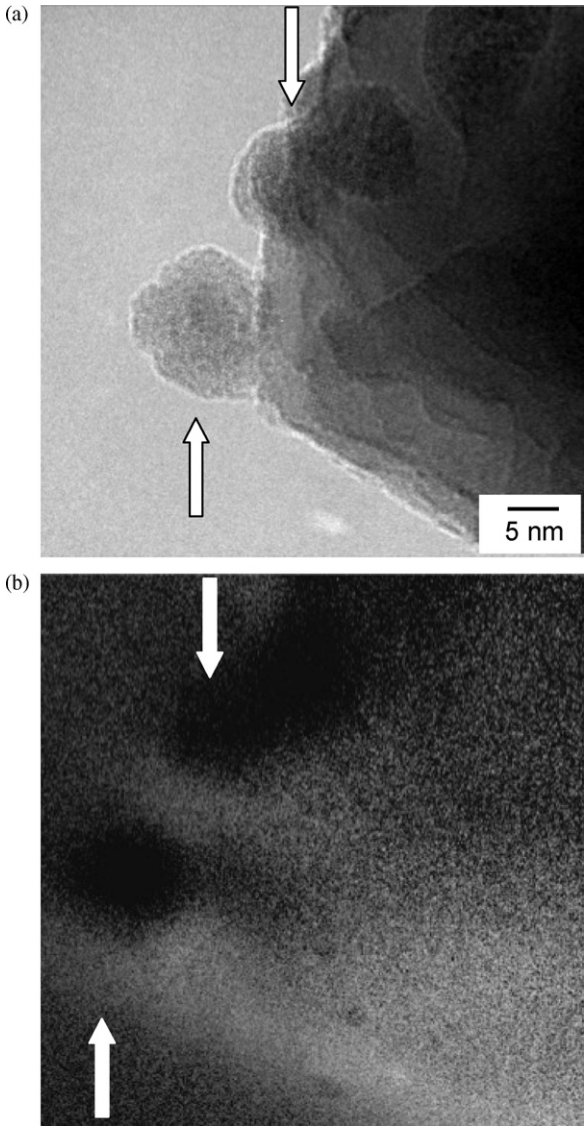

Fig. 8. (a) TEM image and (b) mapping image of Sn atom for 10 wt.% Ru/SnO_2 reduced in 10% H_2/N_2 after pyrolysis at 400 °C in air.

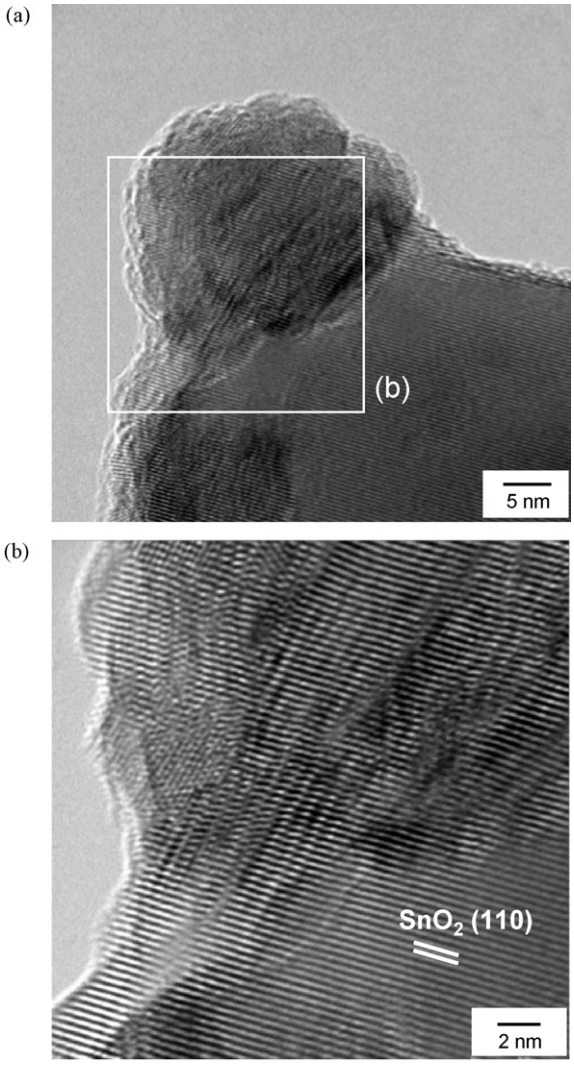

Fig. 9. TEM images of 1.0 wt.% Ru/SnO_2 reoxidized at 400 °C for 0.5 h in air (S-3).

after the exposure to air and the shell part mainly consisted of Sn atom. Therefore, the formation mechanism of the core–shell structure in this Ru/SnO_2 catalyst is the same as that of Pt/SnO_2. According to the surface composition ratio analyzed by XPS and the EELS mapping image of Sn atom, it was confirmed that Sn components were abundant on the surface of the particles in the catalysts exposed to air. These results support the formation mechanism of the core–shell structure mentioned above. In other words, tin species in the particles composed of the intermetallic compound are oxidized in the mild oxidation atmosphere of air, and simultaneously the phase separation of the partially oxidized tin species (SnO_x) proceeds. The formation of intermetallic compounds and subsequent structural change to the core–shell structure should result in the decrease of active sites for the catalytic reaction. In addition, the electronic state of ruthenium species was drastically changed after the reduction treatment as discussed in the previous section. Consequently, the catalytic activity was degraded as shown in Fig. 1.

In the reoxidized catalyst (S-3 and S-4), the particles in the polycrystalline state were clearly observed. The size and shape of the particles in S-3 are similar to those of the particles with the core–shell structure in S-2. This similarity suggests that the particles with the core–shell structure were transformed into the polycrystalline particles by the reoxidation treatment. From the results of XPS analysis, the electronic state of ruthenium species in S-3 and S-4 was assigned to the oxidized state as in the case of S-1. However, the phase ascribable to ruthenium species was not detected by XRD. These results also imply that the drastic change in the microstructure was caused by the reoxidation treatment. In other words, the nano-sized RuO_2 particles were redispersed on the surface of SnO_2 from the particles with the core–shell structure which contained both Ru and Sn atom. In consequence, the catalytic activity was recovered by the reoxidation treatment. However, the activity of S-3 was not comparable to that of S-1 because of the insufficient redispersion by the reoxidation treatment at 400 °C for 0.5 h. The redispersion of precious metal particles has been reported in some catalysts such as Pt/Al_2O_3 [36–38], Pt/MgO [39], $PdO/\alpha\text{-}Al_2O_3$ [40], Rh/CeO_2 [41,42], $Re/\gamma\text{-}Al_2O_3$ [43–45], and Co/SiO_2 [46,47]. The redispersion behavior in Ru/SnO_2 catalyst resembles with that in Pt/SnO_2 catalyst reported previously [11]. In the case of 1.0 wt.% Pt/SnO_2, the reproducibility of the structural changes between particle growth and redispersion was verified [11]. Therefore, the structural changes observed in Ru/SnO_2 catalyst are also expected to be reproducible upon the several reduction–reoxidation treatments. The catalytic activity will be completely restored by choosing the proper condition of the reoxidation treatments.

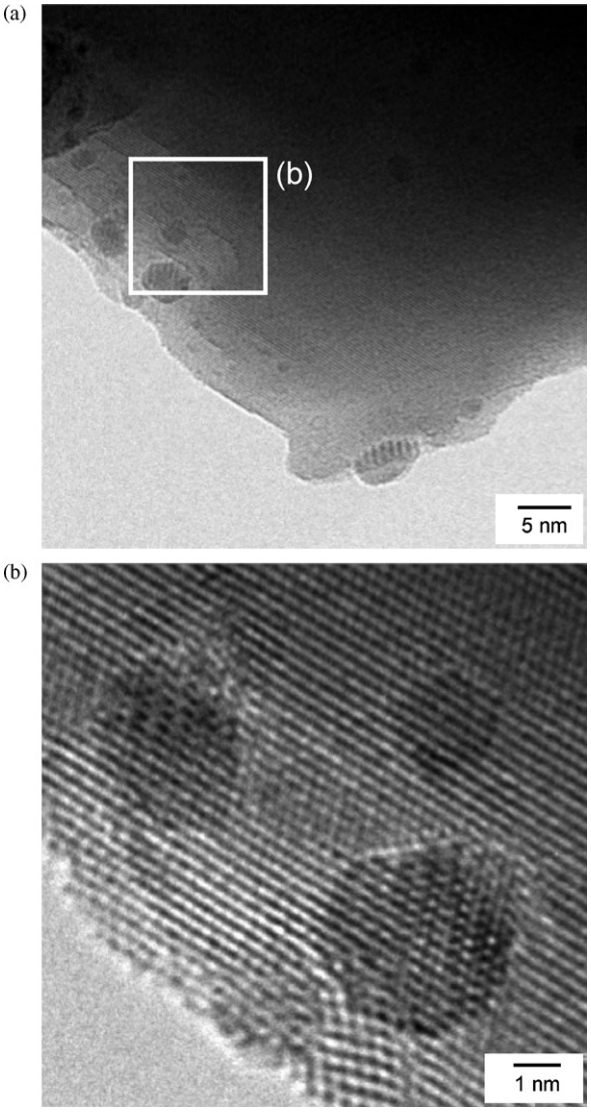

Fig. 10. TEM images of 10 wt.% Ru/SnO_2 reoxidized at 400 °C for 5 h in air (S-4).

4. Conclusions

The correlation between the catalytic activities for ethyl acetate combustion and the microstructure of Ru/SnO_2 catalysts were investigated in detail mainly by TEM observation. It was revealed that the high catalytic activity of the as-calcined catalyst was attributed to the fine and thin RuO_2 particles which possessed the strong chemical interaction with SnO_2 support at the interface. Furthermore, the degradation and restoration of catalytic activities induced by the reduction–reoxidation treatments were also related to the structural changes such as the formation of the particles with core–shell structure and the redispersion of RuO_2 particles. However, the activity and textural structure were not restored completely. Thus, the control of the nano-structure of Ru/SnO_2 catalyst by a suitable pretreatment leads to higher catalytic activity.

Acknowledgment

This work was supported by Core Research for Evolutional Science and Technology (CREST) of Japan Science and Technology Agency (JST).

References

[1] S.J. Tauster, S.C. Fung, R.L. Garten, J. Am. Chem. Soc. 100 (1978) 170.
[2] S.J. Tauster, S.C. Fung, J. Catal. 55 (1978) 29.
[3] S.J. Tauster, In Strong metal support interactions facts and uncertainties, in: R. Baker, S. Tauster, J. Dumesic (Eds.), ACS Symposium Series 298, American Chemical Society, Washington, DC, 1986, p. 1.
[4] S.J. Tauster, Acc. Chem. Res. 20 (1987) 389.
[5] H. Widjaja, K. Sekizawa, K. Eguchi, Chem. Lett. 6 (1998) 481.
[6] H. Widjaja, K. Sekizawa, K. Eguchi, Bull. Chem. Soc. Jpn. 72 (1999) 313.
[7] K. Sekizawa, H. Widjaja, S. Maeda, Y. Ozawa, K. Eguchi, Appl. Catal. A: Gen. 200 (2000) 211.
[8] T. Takeguchi, T. Okanishi, S. Aoyama, J. Ueda, R. Kikuchi, K. Eguchi, Appl. Catal. A: Gen. 252 (2003) 205.
[9] T. Mitsui, K. Tsutsui, T. Matsui, R. Kikuchi, K. Eguchi, Appl. Catal. B: Environ. 78 (2008) 158.
[10] N. Kamiuchi, T. Matsui, R. Kikuchi, K. Eguchi, J. Phys. Chem. C 111 (2007) 16470.
[11] N. Kamiuchi, K. Taguchi, T. Matsui, R. Kikuchi, K. Eguchi, Appl. Catal. B: Environ. 89 (2009) 65.
[12] T. Okanishi, T. Matsui, T. Takeguchi, R. Kikuchi, K. Eguchi, Appl. Catal. A: Gen. 298 (2006) 181.
[13] T. Matsui, K. Fujiwara, T. Okanishi, R. Kikuchi, T. Takeguchi, K. Eguchi, J. Power Sources 155 (2006) 152.
[14] T. Matsui, T. Okanishi, K. Fujiwara, K. Tsutsui, R. Kikuchi, T. Takeguchi, K. Eguchi, Sci. Technol. Adv. Mater. 7 (2006) 524.
[15] T. Matsui, N. Kamiuchi, K. Fujiwara, R. Kikuchi, K. Eguchi, J. Electrochem. Soc. 156 (2009) K128.
[16] M. Scholl, S. Ding, C.W. Lee, R.H. Grubbs, Org. Lett. 1 (1999) 953.
[17] M.S. Sanford, J.A. Love, R.H. Grubbs, J. Am. Chem. Soc. 123 (2001) 6543.
[18] R.H. Grubbs, Tetrahedron 60 (2004) 7117.
[19] P. Kluson, L. Cerveny, Appl. Catal. A: Gen. 128 (1995) 13.
[20] S. Hermans, R. Raja, J.M. Thomas, B.F.G. Johnson, G. Sankar, D. Gleeson, Angew. Chem. Int. Ed. 40 (2001) 1211.
[21] C.J.H. Jacobsen, S. Dahl, P.L. Hansen, E. Törnqvist, L. Jensen, H. Topsøe, D.V. Prip, P.B. Møenshaug, I. Chorkendorff, J. Mol. Catal. A: Chem. 163 (2000) 19.
[22] T.W. Hansen, J.B. Wagner, P.L. Hansen, S. Dahl, H. Topsoe, C.J.H. Jacobsen, Science 294 (2001) 1508.
[23] K. Honkala, A. Hellman, I.N. Remediakis, A. Logadottir, A. Carlsson, S. Dahl, C.H. Christensen, J.K. Nørskov, Science 307 (2005) 555.
[24] K. Yamaguchi, N. Mizuno, Angew. Chem. Int. Ed. 41 (2002) 4538.
[25] J. Barbier Jr., L. Oliviero, B. Renard, D. Duprez, Catal. Today 75 (2002) 29.
[26] S. Hosokawa, H. Kanai, K. Utani, Y. Taniguchi, Y. Saito, S. Imamura, Appl. Catal. B: Environ. 45 (2003) 181.
[27] N. Li, C. Descorme, M. Besson, Appl. Catal. B: Environ. 71 (2007) 262.
[28] T. Mitsui, K. Tsutsui, T. Matsui, R. Kikuchi, K. Eguchi, Appl. Catal. B: Environ. 81 (2008) 56.
[29] A.T. Matveev, A. Kulakov, A. Maljuk, C.T. Lin, H.-U. Habermeier, Physica C 400 (2003) 53.
[30] J.F. Moulder, W.F. Stickle, P.E. Sobol, K.D. Bomben, in: J. Chastain (Ed.), Handbook of X-ray Photoelectron Spectroscopy, Perkin-Ellmer Corporation, Eden Prairie, MN, 1992.
[31] JCPDS File Card No. 040-1290, Joint Committee on Powder Diffraction Standards, Swarthmore, PA.
[32] J. Okal, M. Zawadzki, L. Kepinski, L. Krajczyk, W. Tylus, Appl. Catal. A: Gen. 319 (2007) 202.
[33] X. Shen, L.J. Garces, Y. Ding, K. Laubernds, R.P. Zerger, M. Aindow, E.J. Neth, S.L. Suib, Appl. Catal. A: Gen. 335 (2008) 187.
[34] Y.V. Larichev, B.L. Moroz, V.I. Zaikovskii, S.M. Yunusov, E.S. Kalyuzhnaya, V.B. Shur, V.I. Bukhtiyarov, J. Phys. Chem. C 111 (2007) 9427.
[35] J. Abmann, E. Löffler, A. Birkner, M. Muhler, Catal. Today 85 (2003) 235.
[36] T.J. Lee, Y.G. Kim, J. Catal. 90 (1984) 279.
[37] F.L. Normand, A. Borgna, T.F. Garetto, C.R. Apesteguia, B. Moraweck, J. Phys. Chem. 100 (1996) 9068.
[38] A. Monzon, T.F. Garetto, A. Borgna, Appl. Catal. A: Gen. 248 (2003) 279.
[39] T. Tanabe, Y. Nagai, K. Dohmae, H. Sobukawa, H. Shinjoh, J. Catal. 257 (2008) 117.
[40] K. Narui, H. Yata, K. Furuta, A. Nishida, Y. Kohtoku, T. Matsuzaki, Appl. Catal. A: Gen. 179 (1999) 165.
[41] S. Bernal, J.J. Calvino, M.A. Cauqui, J.M. Gatica, C. Larese, J.A. Perez-Omil, J.M. Pintado, Catal. Today 50 (1999) 175.
[42] S. Bernal, J.J. Calvino, M.A. Cauqui, J.A. Pérez-Omil, J.M. Pintado, J.M. Rodríguez-Izquierdo, Appl. Catal. B: Environ. 16 (1998) 127.
[43] J. Okal, H. Kubicka, L. Kepinski, L. Krajczyk, Appl. Catal. A: Gen. 162 (1997) 161.
[44] J. Okal, L. Kepinski, L. Krajczyk, M. Drozd, J. Catal. 188 (1999) 140.
[45] J. Okal, L. Kepinski, L. Krajczyk, W. Tylus, J. Catal. 219 (2003) 362.
[46] D. Potoczna-Petru, J.M. Jablonski, J. Okal, L. Krajczyk, Appl. Catal. A: Gen. 175 (1998) 113.
[47] D. Potoczna-Petru, L. Kepinski, Catal. Lett. 9 (1991) 355.